Biochimica et Biophysica Acta, 934 (1988) 201–212
Elsevier

BBA 42793

Laser-induced optoacoustic calorimetry of primary processes in isolated Photosystem I and Photosystem II particles

Christian Nitsch, Silvia E. Braslavsky and Günther H. Schatz

Max-Planck-Institut für Strahlenchemie, Mülheim an der Ruhr (F.R.G.)

(Received 4 February 1988)

Key words: Photosynthesis; Electron transport; Optoacoustics; Energy storage; (Cyanobacterium)

The heat released by all primary processes occurring within the first few microseconds after a laser flash of 677 nm was measured by optoacoustic spectroscopy of Photosystem I and II particles isolated from the cyanobacterium *Synechococcus* sp. The heat production was calibrated either 'internally' by inhibiting photochemistry, i.e., closing the reaction centers, or by using solutions of $CuCl_2$ as calorimetric standard. By this method detailed information on the energy partitioning between fluorescence, photochemistry and heat dissipation is obtained for each photosystem. The photoproducts formed within 1.4 ± 0.1 μs in the Photosystem I and II particles, i.e., the states P^+-700 A_1^- and Z^+P-680 IQ_A^-, were found to be associated with a relative energy storage of 0.83 (± 0.08) and 0.65 (± 0.07), respectively. From these data a difference of midpoint potentials (ΔE_m) between P^+-700/P-700 and A_1^-/A_1 of 1520 ± 150 meV was calculated, which implies an $E_m(A_1^-/A_1)$ of $-(1040 \pm 160)$ meV. The midpoint potential difference between Z^+/Z and Q_A^-/Q_A was 1190 ± 100 meV. The consequences for the value of $E_m(Z^+/Z)$ are discussed on the basis of the variability of E_m values reported for the quinone acceptors in the literature. In the case of Photosystem II particles with closed reaction centers a fraction of 5% of the absorbed energy stored for a time longer than 1.4 μs is attributed to the formation of triplet P-680. Data from intact *Synechococcus* cells, excited at 628 and 677 nm, is explained in terms of the results obtained from the isolated particles and the coupling of the antenna pigments in the phycobilisomes to Photosystem II.

Introduction

In a photosynthetic reaction center (RC) the excitation energy absorbed by the antenna pigments is for the most part converted into electrochemical energy of the photoproduct, i.e., a radical pair, which is stabilized by consecutive reactions in the (sub)nanosecond time scale [1]. A smaller fraction is emitted as fluorescence. A third fraction is dissipated as heat during the primary processes. Kinetic and mechanistic information about the primary processes of excitation trapping, charge separation and primary charge stabilization in an RC is provided by fluorescence and absorption studies with picosecond time resolution. The energetics of these processes, i.e., the fraction of energy dissipation and of energy storage, have been usually calculated from equilibrium constants. Those are obtained from midpoint re-

Abbreviations: RC, reaction center; PAS, photoacoustic spectroscopy; LIOAS, laser-induced optoacoustic spectroscopy; PS II, Photosystem II; PS I, Photosystem I; Chl, chlorophyll; Mes, 4-morpholineethanesulphonic acid; EG, ethylene glycol; DCMU, 3-(3,4-dichlorophenyl)-1,1′-dimethylurea; PC, phycocyanin.

Correspondence: S.E. Braslavsky or G.H. Schatz, Max-Planck-Institut für Strahlenchemie, Stiftstraße 34–36, D-4330 Mülheim an der Ruhr, F.R.G.

dox potentials of the respective components involved in the electron-transport chain, or from the analysis of kinetic data (see, e.g., Ref. 2 for a review).

A direct measurement of the energy dissipated as heat is possible with photothermal techniques [3]. Some years ago, conventional photoacoustic spectroscopy (PAS) was introduced to measure the heat evolved in a photosynthetic system upon irradiation with amplitude-modulated continuous light [4]. A gas-coupled microphone was used as detector. This method allowed for the first time in vivo measurements of the photosynthetic energy storage by comparing the heat from a photosynthetically active sample to that obtained from an inhibited sample ('internal' heat calibration) and was applied to intact leaves and cells of algae deposited in layers on filter paper [5,6]. However, since the experimental time window of PAS is in the millisecond-to-second time scale, the heat evolution of the primary and many secondary electron-transfer steps is monitored. It is not possible by this method to obtain information on early intermediates and heat dissipation during the primary processes alone. Furthermore, the PAS signal contains a contribution from 'modulated oxygen evolution', which increases with decreasing modulation frequency. After analysis and separation of this effect [7], PAS in photosynthetic systems is now preferentially applied as an alternative technique to measure electron-transport rates and to monitor processes like Emerson enhancement and state transitions [8,9].

In laser-induced optoacoustic spectroscopy (LIOAS), the heat emitted by a sample after absorption of a short laser pulse is detected as an acoustic pulse by a piezoelectric transducer [10]. The time resolution of the method is determined by the effective acoustic transit time $\tau_a' = 2R/v_a$ that the induced sound pulse in the sample medium takes to cross the laser beam diameter $2R$, where v_a is the velocity of sound [11,12]. For aqueous systems, τ_a' is in the nanosecond-to-microsecond range, depending on the beam diameter. Processes occurring on a longer time scale give no detectable contribution to the signal amplitude. Therefore, LIOAS allows the selective detection of the heat evolved during the formation of early intermediates in the RC.

We have applied the LIOAS method to study selectively the energetics of processes occurring in the Photosystem I (PS I) and Photosystem II (PS II) within a time window of 1.4 ± 0.1 μs. To avoid any interference between both photosystems we used PS I and PS II particles, which were isolated from the cyanobacterium *Synechococcus* sp. We also studied the situation in vivo using intact *Synechococcus* cells. Compared to whole leaves [5,13] and to condensed cell layers [6], the investigation of aqueous suspensions of isolated particles or cells offers also technical advantages: (a) the control of temperature, redox potential and pH in the sample is straightforward; (b) the control of pigment concentration and of photon density is possible; (c) the acoustic coupling of the photosynthetically active protein complexes to the medium is improved and the signal contribution from scattered light is significantly reduced; (d) for homogeneous suspensions the heat production of the system can be calibrated not only 'internally' (see above) but also 'externally' using a $CuCl_2$ reference solution (see Materials and Methods). Thus, a detailed picture can be gained for the energy distribution between fluorescence, photochemistry and heat dissipation associated with all the processes occurring within a few μs for both Photosystems I and II.

Materials and Methods

Samples

Cells of the thermophilic cyanobacterium *Synechococcus* sp. (obtained from Prof. S. Katoh, University of Tokyo, Komaba, Meguro-Ku, Tokyo 153, Japan) were grown under conditions given in Ref. 14. From this species oxygen-evolving PS II particles with a ratio of about 80 Chl/P-680 were isolated using the detergent sulfobetaine 12 according to Ref. 15. From the resulting PS II-lacking membrane fragments PS I particles with about 100 Chl/P-700 were isolated by a further detergent treatment with Triton X-100 (Schatz, G.H., unpublished data).

The PS I particles were suspended in 50 mM phosphate buffer (pH 7) containing 0.1% (w/w) Triton X-100. The PS II particles were suspended in a buffer solution (500 mM sucrose, 10 mM $MgCl_2$, 2 mM K_2HPO_4, 5 mM $CaCl_2$ and 10

mM Mes-NaOH (pH 6)). Samples containing intact cells were directly taken from the *Synechococcus* cultures. In order to obtain larger optoacoustic signals the buffer solutions were diluted with 33% (v/v) ethylene glycol (EG). The amplitude of the pressure pulse is directly proportional to the ratio β/c_p of the medium [10] (β is the cubic expansion coefficient, c_p is the specific heat capacity); EG is a convenient additive, since the value of β/c_p for EG is about 5-times larger than that for water [17]. Addition of EG did not affect the electron transport from water to $K_3Fe(CN)_6$ in PS II particles. Measurement of $K_3Fe(CN)_6$ reduction under saturating continuous red light ($\lambda > 630$ nm) showed no difference between samples with and without 33% EG. The Chl concentration for all samples was about 5–6 μM and the absorbance at 677 nm due to Chl was about 0.4.

By inhibition of the photosynthetic activity an internal calibration for maximum heat production can be obtained for each photosystem, since no energy is stored by secondary products under these conditions [4]. The RCs of the PS I particles were kept open by adding 1 mM sodium ascorbate and dark adaptation, and were closed by oxidation of P-700 upon adding 1 mM $K_3Fe(CN)_6$ and background illumination ($\lambda_{exc} > 695$ nm, 300 $W \cdot m^{-2}$). The RCs of the PS II particles were kept open by adding 1 mM $K_3Fe(CN)_6$ and dark adaptation, and were closed by reducing the primary quinone acceptor Q_A upon adding 50 μM DCMU or 2 mM dithionite and white background illumination (1500 $W \cdot m^{-2}$, 400–720 nm). In the intact cells the RCs were closed by white background light (1500 $W \cdot m^{-2}$, 400–720 nm) and addition of 50 μM DCMU.

$CuCl_2 \cdot 2H_2O$ (Merck z.A.), dissolved in a 1 : 2 (v/v) EG/water mixture was used as an independent calorimetric standard [18].

Apparatus

The LIOAS set-up was similar to the one described in Refs. 12 and 19 with the following changes.

(a) A 15-ns pulse from an excimer-pumped dye laser (Lambda Physics) at a repetition rate of 1 Hz was used for excitation at 628 and 677 nm (DCM or Pyridine 1 as laser dyes in methanol, Lambda Physics). The laser beam diameter $2R$ was varied with several pinholes between 0.4 and 6 mm, corresponding to effective acoustic transit times τ_a' in the EG/water mixture between 270 ns and 4.5 μs [19]. For diameters above 1 mm the beam was expanded by two convex lenses ($f = 25$ and 40 mm) before passing through the pinhole. The laser output energy was varied by means of neutral density filters between 70 nJ and 35 μJ per pulse. At our standard condition at $2R = 2$ mm ($\tau_a' = 1.4 \pm 0.1$ μs) and $\lambda = 677$ nm this corresponds to excitation energy densities ranging from 3 μJ per cm^2 per pulse to 3 mJ per cm^2 per pulse or fluences ranging from 10^{13} photons per cm^2 per pulse to 10^{16} photons per cm^2 per pulse. For PS II particles with 80 Chl/RC, 0.07–70 photons/RC are absorbed under our conditions (5 μM Chl).

(b) The samples were thermostated at 17 °C in an external reservoir and pumped (20 ml/min) through a 1-cm pathlength cuvette in order to replace the irradiated sample volume after every laser pulse and to prevent sedimentation of the intact cells. The reservoir could be illuminated by the appropriate background light (fiber optics, Oriel 77501) as specified above.

(c) In order to increase the signal-to-noise ratio at low pulse energies a combination of two 4 mm thick, 400 kHz piezoelectric transducers (PZT ceramic, Vernitron) attached to opposite walls of the flow cuvette was used. If the laser beam passes exactly through the middle of the cuvette the signals from both detectors are in phase and can be superimposed. They were added (Tektronix 7A12) and further amplified, averaged (100 ×) and energy-normalized as described [19]. The signal trace that is due to the ringing of the piezoceramic (Fig. 1) was independent on beam diameters between 0.4 and 2 mm; however, widening up the beam to 6 mm diameter led to a significant broadening and decreasing of the expansion and contraction peaks. Nonresonant piezoelectric films [12,19] could not be used here, since they are less sensitive than the ceramic elements [20].

(d) An additional signal contribution due to scattered-light absorption by the detectors was observed as a small shoulder prior to the first peak when using intact cells (size, approx. 5 μm) (Fig. 1a). To correct for this artefact, signals only due to scattered light were generated with emulsions of phospholipids in EG/water mixtures of matched

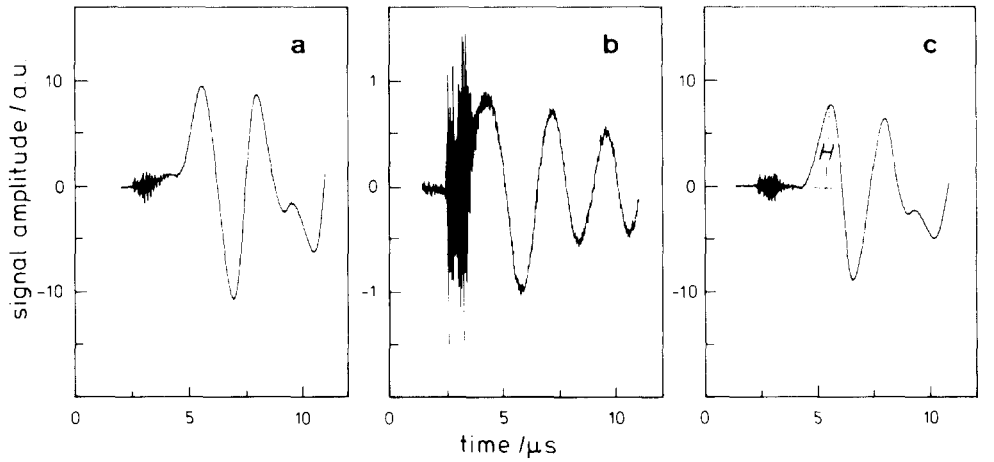

Fig. 1. Signal traces (λ_{exc} = 677 nm, beam diameter $2R$ = 0.9 mm, E_0 = 5 μJ, single shot) obtained from (a) an EG/buffer solution containing intact cells and (b) a phospholipid emulsion in a EG/water mixture. Note the tenfold expansion of the scale in (b). The turbidities were matched by comparing the absorbances at 750 nm. (c) Difference between signal (a) and signal (b).

turbidity at 750 nm (Fig. 1b). They were substracted from the measured signals in order to obtain the corrected signals originating only from the absorption of the excitation light by the sample (Fig. 1c). This procedure is as used in an earlier LIOAS study of intact leaves [13]. However, the scattered-light signals from cells were generally one order of magnitude smaller than those from leaves. No scattered light-induced signals were detected from PS II and PS I particles which are known to have diameters less than 20 nm [21]. Sample absorbances were measured with a Perkin-Elmer 356 spectrophotometer in a compartment close to the end-on photomultiplier tube.

Signal amplitudes from samples with open and closed RCs were measured over a wide energy range (see above). Intact cells and PS II particles were excited with 628 and 677 nm, the absorption maxima of phycocyanin (PC) and Chl *a*, respectively. PS I particles were excited at 677 nm only.

Heat calibration

For a dilute sample the voltage amplitude H of the optoacoustic signal (Fig. 1c) is given by Eqn. 1 [10,20]

$$H = K\alpha E_0(1-10^{-A}) \tag{1}$$

where K is a proportionality factor containing apparative, geometrical and thermoelastic parameters, E_0 the incident excitation energy, A the sample absorbance and α the fraction of the absorbed energy that is dissipated as heat within the effective acoustic transit time τ_a' [11,22]. For a calorimetric standard like $CuCl_2$, which releases all energy absorbed by 'prompt' thermal deactivation processes within a few nanoseconds, α is equal to unity [18]. For a sample in which some energy is stored by products for a time longer than τ_a' or lost by fluorescence, α becomes less than 1 and the slope of a plot of H vs. E_0 is proportionally decreased. Internal heat calibration in photosynthetic systems can be achieved by measurements on closed RCs at the same sample absorbance and excitation energy as that used for the open RCs [5]. Then, α is obtained according to Eqn. 2 from the ratio of the signal amplitudes of samples with open RCs, H^{op}, and closed RCs, H^{cl}. The latter is corrected for fluorescence:

$$\alpha = \left(1 - \Phi_f^{cl}\frac{\nu_f}{\nu_e}\right)\frac{H^{op}}{H^{cl}} \tag{2}$$

Φ_f^{cl} denotes the fluorescence quantum yield for closed RCs. ν_e and ν_f are the radiation frequencies of excitation and the weighted average of fluorescence, respectively. For PS II $\nu_f/\nu_e = 0.99$ is obtained. For PS I this ratio is somewhat smaller, but since Φ_f^{cl} for PS I is negligible (vide infra), the first term in Eqn. 2 becomes unity for PS I.

Curve fitting

Computer fits of the energy-dependencies of the normalized optoacoustic signals according to Eqn. 3 (vide infra) were performed by a nonlinear least-square optimization program (Levenberg-Marquardt algorithm).

Results and Discussion

Signal energy dependence

In Fig. 2 the signal amplitude H from PS I particles (with 1 mM sodium ascorbate) for a laser beam diameter of 2 mm ($\tau_a' = 1.4$ μs) and a laser wavelength of 677 nm is plotted vs. the pulse energy E_0. Around $E_0 = 1$ μJ a significant increase in the slope is observed. For comparison, a plot of H vs. E_0 for a $CuCl_2$ solution with the same absorbance at 677 nm and under the same geometrical conditions is shown in the same figure. A straight line passing line through the origin results for this standard. Its slope does not change even at higher energies (more than 30 μJ, not shown) and represents the maximum prompt heat production.

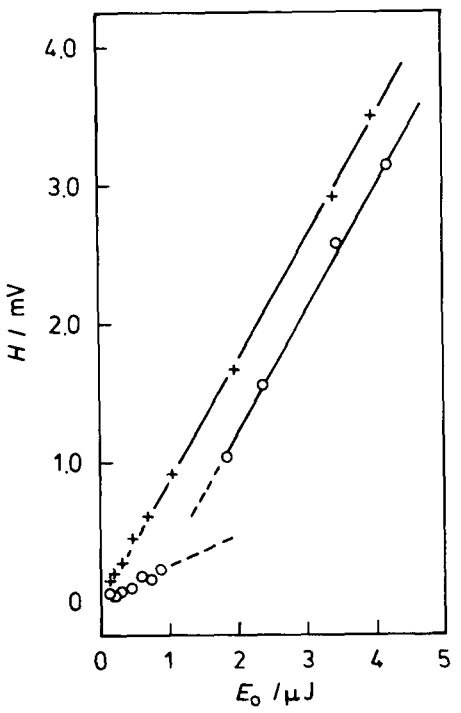

Fig. 2. Amplitude H of the signal peak plotted vs. the laser energy E_0 (○) for an EG/buffer solution containing PS I particles with 1 mM sodium ascorbate and (+) for a $CuCl_2$ solution at matched absorbance at $\lambda_{exc} = 677$ nm; $2R = 2$ mm.

According to Eqn. 1 the change of the slope H/E_0 for the PS I particles from an initial small to a higher value with increasing laser energy means that a smaller fraction of the absorbed energy is stored under the latter condition. This can be explained by a closure of the RCs by the excitation light. Since the laser pulses used have a duration of approx. 15 ns FWHM, the probability of double hits of the RCs at high laser energies is not negligible. A change in the H/E_0 slope was already observed during the optoacoustic studies of leaves at pulse energies above 1 μJ but could not be well resolved [13]. Owing to the improved sensitivity of our present detection system and the better acoustic coupling of the photosynthetic membranes to the medium we were able to decrease the pulse energy far below 1 μJ. By additional expansion of the laser beam to a diameter above 1 mm the fluence was further reduced so that an average of less than one photon per RC was absorbed and double hits were negligible. Thus, the flat slope obtained at low energies corresponds to the heat released from open RCs, while the steeper one at high energies to that from closed RCs, respectively. In the following the symbols H^{op} and H^{cl} denote the signal amplitudes from RCs which had been opened and closed, respectively, prior to the measurement by chemical and photochemical treatment. This terminology is maintained in each case over the entire fluence range. Thus, H^{op} denotes also signal amplitudes from RCs which were closed by laser pulses with high fluence. With every system studied a change in the value of the slope H^{op} vs. E_0 was obtained.

We prefer to show here semilogarithmic plots of the energy-normalized signals H_N^{op} ($= H^{op}/E_0$) vs. the pulse energy E_0. Such a plot should exhibit an inflexion point separating two H_N^{op} levels: a lower one, representing the thermal loss under conditions where each photon absorbed in the antenna initiates a charge separation in the RC (at the low energy limit), and a higher one representing the maximum heat production by the RCs closed by the excitation light itself (at the high energy limit). The 'true' value of H_N^{op} is the value obtained at low energies.

PS I particles

In Fig. 3 a semilogarithmic plot of H_N^{op} vs. E_0 for PS I particles and $\lambda_{exc} = 677$ nm at different laser beam diameters $2R$ is shown. The complete inflexion behavior can be observed only for $2R = 2$ mm, i.e., at the lowest fluence. Decreasing the beam diameter from 2 to 0.4 mm, i.e., increasing the fluence by a factor of 25, results in a proportional shift of the inflexion point on the log E_0 axis (from approx. -5.7 to approx. -7.0). This shift clearly demonstrates the energy-dependent closure of the RCs by multiple hits. For all diameters the pulse energy at the inflexion point corresponds to a fluence of approx. 60 μJ per cm^2 per pulse or to approx. 1.5 photons per RC. No mathematical fitting was performed for the points, since these experiments should only illustrate the variation of the inflexion point with the beam diameter. Thus, opposite to Fig. 4 (vide infra) the solid curves were drawn by hand.

In Fig. 4 the values of H_N^{cl} from PS I particles

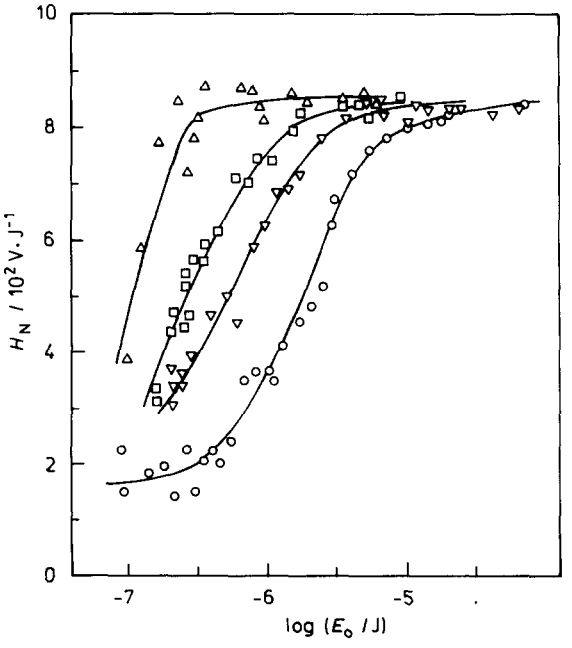

Fig. 3. Energy-normalized LIOAS signals H_N^{op} from PS I particles (with 1 mM sodium ascorbate) at $\lambda_{exc} = 677$ nm for various laser beam diameters ($2R$) plotted vs. the logarithm of the laser energy E_0. $2R = 0.4$ mm (△), 0.9 mm (□), 1.5 mm (▽), and 2.0 mm (○). The solid curves are drawn by hand.

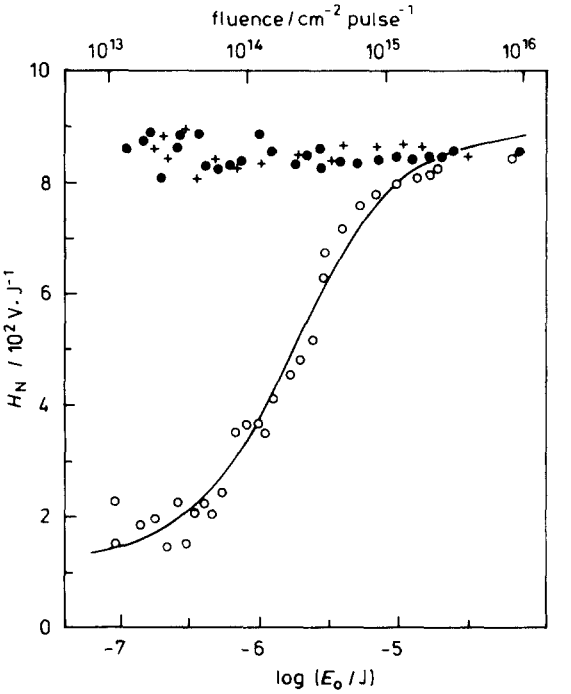

Fig. 4. Energy-normalized LIOAS signals H_N from PS I particles (○) with 1 mM sodium ascorbate (data from Fig. 3) and (●) with 1 mM $K_3Fe(CN)_6$, and from a $CuCl_2$ solution (+); $2R = 2.0$ mm ($\tau_a' = 1.4$ μs). Absorbances matched at $\lambda_{exc} = 677$ nm. The solid curve represents a Poisson fit according to Eqn. 3 with $A = 1.2 \cdot 10^2$ V·J^{-1}, $B = 7.6 \cdot 10^2$ V·J^{-1} and $C = 0.9$ μJ^{-1}.

with chemically preoxidized RCs (P^+-700), in which the charge separation P^*-700$A_1 \rightarrow P^+$-700A_1^- is not possible, are compared to the corresponding H_N^{op} values. For the samples with inhibited charge separation an energy-independent H_N^{cl} value identical with the H_N^{op} level at high E_0 was observed. Since Φ_f^{cl} is negligible for PS I (approx. 0.002 (Schatz, G.H., unpublished data)), the internal calibration for PS I is equivalent to the total transformation of the absorbed energy into heat. This was confirmed by the coincidence of the H_N^{cl} values with the energy-normalized signals from a $CuCl_2$ reference solution over the entire E_0 range (Fig. 4). It can also be seen from the original plots of H vs. E_0 in Fig. 2. At low energies $H_N^{op}/H_N^{cl} = 0.25$ and with Eqn. 2, $\alpha = 0.25$ were obtained for PS I particles (see Table I).

The energy-dependence of the H_N^{op} values was fitted to a cumulative one-hit Poisson distribution [23] according to Eqn. 3:

$$H_N = A + B\left(1 - \frac{1 - e^{-CE_0}}{CE_0}\right) \quad (3)$$

The parameter C is related to the unit absorption cross section. From the result of the optimal fit (solid curve in Fig. 4), i.e., $C = 0.9\ \mu J^{-1}$ and the Chl absorption cross section $\sigma = 1.6 \cdot 10^{-16}$ cm^2 at 677 nm a value of 0.8 photons per 100 Chl, i.e., approx. 1 photon per RC is calculated. This point, corresponding to e^{-1} of the amplitude B, defines the beginning closure of the RCs by double and multiple hits within the 15 ns laser pulse with increasing fluence. The parameter A is used as H_N offset at low fluence.

PS II particles. Effect of singlet–singlet annihilation and triplet P-680 formation

The energy dependence of the signals for the PS II particles excited at 677 nm and with a beam diameter of 2 mm ($\tau_a' = 1.4 \pm 0.1$ μs) was quite different from that for the PS I particles. Again the energy-normalized signals, H_N^{op}, strongly increase with pulse energy, up to the values for PS II particles with closed RCs, H_N^{cl} (Fig. 5). However, no plateau for H_N^{op} at high E_0 is reached. The values for closed RCs, H_N^{cl}, are nearly constant at low energies but increase significantly at higher E_0, following a sigmoidal curve. The inflexion region corresponds to energy densities between approx. 40 μJ per cm per pulse and 80 μJ per cm per pulse, i.e., to 1–2 photons absorbed per RC. By variation of the laser beam diameter this region can be shifted on the log E_0 axis in the same way as it was observed for the inflexion point of the H_N^{op} curves for the PS I particles (see above).

For closed RCs, i.e., a system that does not react photochemically, an energy-dependent enhancement of the heat production can be understood in terms of a decrease of the concurrent process, i.e., fluorescence. A decrease of the fluorescence quantum yield and a shortening of the fluorescence lifetime are known to occur at high fluences in photosynthetic units as a consequence of singlet–singlet annihilation according to

$$^1Chl^* + {}^1Chl^* \rightarrow {}^1Chl^* + {}^1Chl + heat$$

This effect was studied, e.g., with purple bacteria, using picosecond flashes [24] and with *Chlorella*, using nanosecond flashes [23] of increasing intensities. With the same PS II particles as those used in this work, picosecond studies have shown that singlet–singlet annihilation becomes important at fluences corresponding to more than 0.2 photons per RC [25]. In the LIOAS experiment described in this work the threshold fluence is about one order of magnitude higher (1–2 photons per RC). This apparent difference is explained by the different laser pulse widths used, since completely different fluence dependencies of the annihilation effect are expected for pulse durations shorter and longer than the average exciton lifetime. While in Ref. 25 pulses of approx. 10 ps FWHM were used, being much shorter than the average exciton lifetime, in the LIOAS experiment the excitation energy is distributed over a laser pulse of approx. 15 ns FWHM, i.e., a time interval much longer than the average exciton lifetime.

Using $CuCl_2$ as reference solution under the same experimental conditions as for the PS II particles the energy-normalized signals showed constant H_N values over the whole energy range (Fig. 5). At high E_0 the H_N^{cl} signals (error less than 1%) from the PS II particles approach the $CuCl_2$ signal level. This means that under these conditions Φ_f^{cl} approaches zero owing to almost complete annihilation of the Chl singlet states. At lower E_0 (signal error, approx. 5%) the difference between the $CuCl_2$ signals and the H_N^{cl} signals is about 10–15%. Φ_f^{cl} for the PS II particles used here is known to be in the order of 0.05–0.1 [25]. Hence, a fraction of (5 ± 5)% of the absorbed energy is neither released as fluorescence nor detected as heat within τ_a' (1.4 ± 0.1 μs for $2R = 2$ mm) at low energies. However, also this fraction is converted to heat at high energies, where no signal difference between $CuCl_2$ and PS II particles is observed. Thus, for PS II an energy-independent internal heat calibration cannot be obtained. This result can be explained by (a) the energy-dependent fluorescence quantum yield and (b) a partial deactivation of the reduced state P^+-680$I^-Q_A^-$ of closed RCs in PS II via triplet P-680 [26], which is formed 'promptly' (in nanoseconds) but decays to the ground state in a time longer than the experimental time window (in microseconds). About 5%

of the absorbed energy are stored by such a process at low excitation energies. This must be taken into account in the calculation of α at low energies, in addition to the correction for the fluorescence in Eqn. 2. Under the rough assumption that the triplet energy content is close to that of the first excited singlet, the triplet yield can be estimated to be in the range of $(5 \pm 5)\%$. At high fluences nearly the whole energy absorbed by the antenna Chls is dissipated by prompt thermal deactivation processes, since singlet–singlet annihilation becomes dominant compared to exciton trapping (i.e., charge separation and eventual triplet P-680 formation). Therefore, no difference is observed for the 'energy-normalized heat production', H_N, between $CuCl_2$ and closed PS II at high energies. At low energies $H_N^{op}/H_N^{cl} = 0.45$ and $\alpha = 0.4$ were obtained for the PS II particles at 677 nm (see Table I).

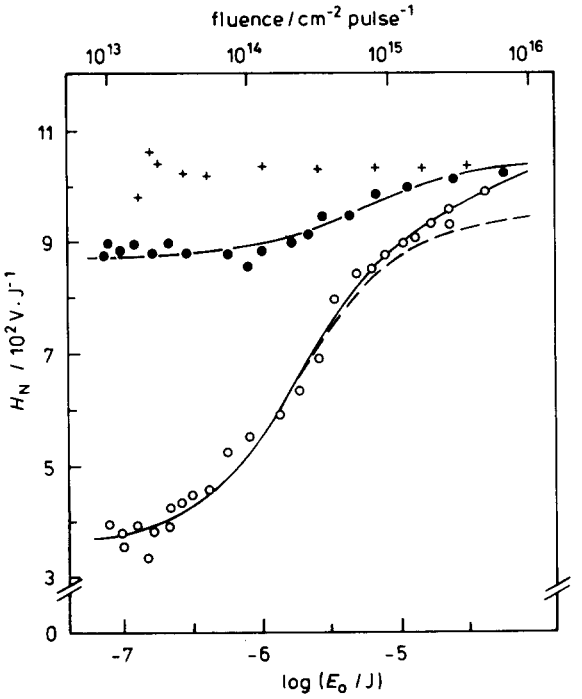

Fig. 5. Energy-normalized LIOAS signals H_N from PS II particles (○) with 1 mM $K_3Fe(CN)_6$, (●) with 2 mM dithionite, and from a $CuCl_2$ solution (+); $2R = 2.0$ mm ($\tau_a' = 1.4$ μs). Absorbances matched at $\lambda_{exc} = 677$ nm. The upper solid curve is a Poisson fit according to Eqn. 3 with $A = 8.74 \cdot 10^2$ V·J^{-1}, $B = 1.61 \cdot 10^2$ V·J^{-1} and $C = 0.3$ μJ^{-1}. The lower solid curve is the sum of two fits according to Eqn. 3, one with $A = 3.5 \cdot 10^2$ V·J^{-1}, $B = 5.9 \cdot 10^2$ V·J^{-1}, $C = 0.95$ μJ^{-1} (dashed curve) and a second one with $A = 0$, $B = 0.9 \cdot 10^2$ V·J^{-1} and $C = 0.04$ μJ^{-1} (not shown).

The above explanations of the signal energy-dependence for PS II particles are supported by computer fits of the H_N^{cl} and H_N^{op} values. The upper solid curve in Fig. 5 (H_N^{cl}) again is a Poisson fit according to Eqn. 3. It corresponds to the so-called 'Poisson saturation' [23] and describes the gradual decrease of the fluorescence quantum yield for closed RCs (F_{max}) with increasing fluence. It should be noted, however, that the H_N^{cl} values are not only related to the fluorescence quantum yield Φ_f^{cl} but also reflect the energy storage by the triplet P-680 as described above. From the fit $C = 0.3$ μJ^{-1} is obtained, which corresponds to 2.2 photons per 100 Chl, i.e., approx. 1.8 photons per RC in the PS II particles, at Be^{-1}. The lower solid curve (H_N^{op}) is the sum of two fitted components according to Eqn. 3. The first component (dashed curve) represents the H_N^{op} energy dependence, neglecting fluorescence and taking into account the fraction (5%) of energy that is stored by the triplet P-680 in closed RCs at low fluence but contributes to the 'energy-normalized heat production' at high fluence. For this reason, the high fluence plateau of the dashed curve is somewhat higher than the low fluence plateau of the H_N^{cl} fit. $C = 0.95$ μJ^{-1} is obtained for the dashed curve, which compares well to the value for the PS I particles (0.9). This was to be expected, since the antenna sizes for both particles are similar. For the second component (not shown) $C = 0.04$ μJ^{-1} is obtained, corresponding to approx. 13 photons/RC at $B \cdot e^{-1}$. This component, shifted towards lower fluence by one order of magnitude compared to the H_N^{cl} fit, may reflect the S–S annihilation in photosynthetic units with the RCs in the open state prior to the measurement [23,24]. It should be noted that also the second component was obtained by a 'singlet-hit' Poisson distribution and not by a 'multiple-trap' function as postulated in Ref. 23. However, such details, also considering the different values of F_0 and F_{max}, cannot be obtained from our data, since the fluorescence yield was not directly measured, but rather represents one of the contributions to the optoacoustic signal.

Calorimetric evaluations for PS I and PS II particles

Provided no closure of the RCs by the laser pulse occurs, the fraction of heat dissipated promptly, α, can be used to calculate the relative storage by the photoproducts formed within the effective acoustic transit time τ_a' (see Table I). α is related to the product of the quantum yield of the photoreaction, Φ_r, and the molar energy content of the photoproduct, ΔE_r, by simple energy balance considerations [4,18]

$$N_A h\nu_e = \alpha N_A h\nu_e + \Phi_f^{op} N_A h\nu_f + \Phi_r \Delta E_r \quad (4)$$

N_A is the Avogadro number, h the Planck constant, and Φ_f^{op} denotes the fluorescence quantum yield for open RCs. α is obtained from Eqn. 2. Rearrangement of Eqn. 4 leads to Eqn. 5:

$$\frac{\Delta E_r}{N_A h\nu_e} = \frac{1 - \alpha - \Phi_f^{op}}{\Phi_r} \quad (5)$$

The relative energy storage ($\Delta E_r/N_A h\nu_e$) by the photoproduct formed in PS I particles within 1.4 μs was calculated as follows.

Using $H_N^{op}/H_N^{cl} = \alpha = 0.25$ and $\Phi_f^{op} = \Phi_f^{cl} = 0.002$, and assuming $\Phi_r = 0.9$, $\Delta E_r/N_A h\nu_e = 0.83$ (± 0.08) was obtained (Table I). From this it follows that about 20% of the absorbed light energy are released by fast stabilization processes within τ_a' (1.4 μs for $2R = 2$ mm), whereas about 80% remains stored in the system. This time window includes the charge separation between P-700 and A_1 [27]:

$$P^*\text{-}700A_1 \rightarrow P^+\text{-}700A_1^-$$

The subsequent electron-transfer steps to the ferredoxin acceptors F_X, F_A and F_B and to the secondary donors of PS I occur in the micro-to-millisecond time range and are not monitored by our experiment.

The relative energy storage by the photoproduct formed in PS II particles was calculated analogously: an α value of 0.4 is obtained from $\Phi_f^{cl} = 0.07$ and $H_N^{op}/H_N^{cl} = 0.45$ (which is reduced by 5% correcting for the energy stored by triplet P-680 for a time longer than 1.4 μs). With $\Phi_f^{op} = 0.02$ and a quantum yield for charge stabilization in open PS II, $\Phi_r = 0.9$ [37], a value of $\Delta E_r/N_A h\nu_e = 0.65$ (± 0.07) is calculated (Table I). This means that about one-third of the absorbed light energy is released by fast stabilization processes within 1.4 μs and about two-thirds remain stored in the system. According to known kinetic data [1,25,29] for the electron-transport chain in PS II this time window includes the charge separation processes which yield the secondary radical pair Z^+P-680IQ$_A^-$ according to

$$ZP^*\text{-}680IQ_A \xrightarrow{80\ ps} ZP^+\text{-}680I^-Q_A \xrightarrow{500\ ps} ZP^+\text{-}680IQ_A^-$$

$$\xrightarrow{> 25\ ns} Z^+P\text{-}680IQ_A^-,$$

where I is a pheophytin, the primary electron acceptor, Q_A the first quinone acceptor, and Z the secondary donor in PS II. A comparison of the $\Delta E_r/N_A h\nu_e$ values obtained for PS I and PS II particles shows that the energy loss in the forward electron transfer in the RCs of PS I (approx. 20%) is only about half of that in the RCs of PS II (approx. 35%). This result can be rationalized by comparing the number of components and electron-transfer steps involved in the formation of the radical pairs within 1.4 μs in both photosys-

TABLE I

Fraction of energy-normalized signal amplitudes, H_N^{op}/H_N^{cl}, prompt heat dissipation, α, relative energy storage by photoproducts, $\Delta E_r/N_A h\nu_e$, and difference between midpoint potentials of the components, ΔE_m, obtained for PS I particles, PS II particles and intact cells at different excitation wavelengths, λ_{exc}

	λ_{exc} (nm)	H_N^{op}/H_N^{cl}	α	$\Delta E_r/Nh\nu_e$	ΔE_m (meV)
PS I particles	677	0.25	0.25	0.83	1520
PS II particles	677	0.45	0.4	0.65	1190
Intact cells	628	0.4	–	–	–
	677	0.65	–	–	–

tems: while in PS I the positive charge remains on the primary donor, it is further stabilized in PS II on the donor Z. An increase of heat production with the number of electron-transfer steps involved in the photosynthetic charge separation is expected, since each step is associated with a free-energy decrease. An experimental condition to monitor also radical pair states with P^+-680 demands for a transit time in the range within some tens of nanoseconds. So far, it is not possible to obtain calorimetric informations about processes occurring in the picosecond-to-nanosecond range by the LIOAS method, e.g., the primary charge separation and stabilization in PS II. Recently, LIOAS was applied to measure lifetimes of species down to 60 ns using laser beam diameters below 1 mm or even focussed beams [12,19,30]. As shown above, the decrease of the beam diameter is limited to 2 mm ($\tau_a' = 1.4$ μs) for photosynthetic systems. With smaller diameters, affording smaller time windows, the pulse energy must be decreased far below 100 nJ in order to avoid closing of the RCs. Even with our improved detection using two piezoceramic elements reliable signals could not be obtained at these low energies.

In order to increase the time window to its highest possible value, we expanded the laser beam to a 6 mm diameter, which corresponds to $\tau_a' = 4.5$ μs. Only PS II particles were measured and no change in H_N^{op}/H_N^{cl} relative to the smaller time window (1.4 μs) was observed. This was to be expected, since all secondary reactions in these PS II particles, i.e., Z^+ reduction by the water-splitting system complex and Q_A oxidation by Q_B, are known to occur in the time range from 30 μs to several ms [31]. Hence, there is no contribution by such secondary processes to the heat production in LIOAS. This method is therefore a powerful tool to monitor exclusively the primary steps in the photosynthetic electron-transport chain.

Intact cells

For intact cells, excited at 677 nm (Chl absorption), the same type of energy-dependence as for PS I particles was observed (not shown) for the scattering-corrected and energy-normalized signals H_N^{op} and H_N^{cl}. This is expected, since excitation at 677 nm mainly activates PS I (vide infra). However, excitation with 628 nm (phycobiliprotein absorption) yielded energy-dependent signals H_N^{op} and H_N^{cl} as observed for the PS II particles (not shown). This is consistent with findings that the energy absorbed by the phycobiliproteins in phycobilisomes is preferentially transferred to the Chl antenna of PS II with high efficiency. At low energies H_N^{op}/H_N^{cl} values of 0.4 and 0.65 at 628 and 677 nm, respectively, were obtained (Table I).

Comparison between isolated particles and intact cells

By comparing H_N^{op}/H_N^{cl} from PS I and PS II particles to those from intact cells further information can be obtained about the role and interaction of the two photosystems:

Internal heat calibration for the intact cells was obtained by adding DCMU, which leads to an accumulation of Q_A in its reduced state, thus closing the RCs of PS II. The PS I/PS II ratio in *Synechococcus* is about 3:1, and Chl/RC I > Chl/RC II, i.e., excitation at 677 nm (Chl) activates mainly PS I. Under the assumption that the electron transport to PS I is totally inhibited in the presence of DCMU, one should obtain for the cells at 677 nm an H_N^{op}/H_N^{cl} value close to that from isolated PS I particles (at least 0.25). Alternatively, a value close to unity would be expected if only PS II is inhibited by DCMU and background white illumination. In fact, the obtained value of 0.65 indicates that PS I is only partially affected by the inhibition procedures. This may be due to an electron-transfer pathway to P^+-700 which is not dependent on PS II as electron source. A very rapid electron donation to P^+-700 in *Synechococcus* is known to occur from cytochrome *c*-553 and cytochrome *f* [32].

A lower fraction of the absorbed energy released as heat was observed at 628 nm (0.4) than at 677 nm (0.65) for intact cells. Since the procedures for internal heat calibration in vivo mainly affect PS II, the data indicate that a higher proportion of energy absorbed at 628 nm than that absorbed at 677 nm is used for PS II photochemistry. The fact that the values obtained for isolated PS II particles at 677 nm (0.45) and for intact cells at 628 nm (0.4) are similar again is consistent with an efficient energy transfer from the phycobiliproteins to PS II in vivo.

Conclusion

With the assumption that the entropy changes due to the electron-transfer processes are small as compared to the enthalpy changes, we can estimate the standard free energy levels of the states formed within our time window of 1.4 μs. Based on this assumption and neglecting the Coulombic interactions between the charged donors and acceptors as a first approach one can convert the relative energy storage $\Delta E_r/N_A h\nu_e$ into a corresponding value of midpoint-potential difference, ΔE_m, between the components involved (Table I and Fig. 6).

A value of $E_m(A_1^-/A_1) = -(1040 \pm 160)$ meV is derived for PS I particles from the experimental energy storage of 83% (corresponding to $\Delta E_m =$ 1520 meV) and the mean $E_m(P^+\text{-}700/P\text{-}700)$ of 480 meV (see Ref. 1 for a review). The obtained

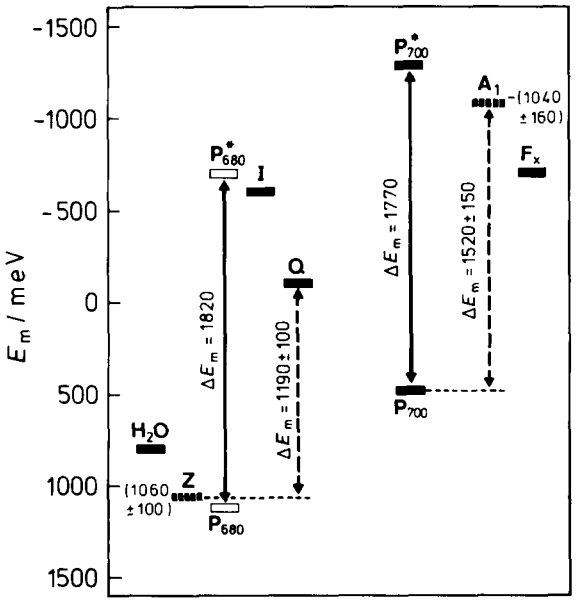

Fig. 6. Energetic scheme of components involved in the electron-transport processes in PS II and PS I leading to the formation of the radical pairs Z^+ P-680IQ_A^- and P^+-700A_1^-, respectively. P-680 is the primary donor, I the primary acceptor, Q the first quinone acceptor, and Z the secondary donor in PS II. P-700 is the primary donor, A_1 the primary acceptor and F_X the first ferredoxin acceptor in PS I. Closed rectangles and full lines correspond to known data, whereas open rectangles denote estimated data. Striped rectangles and broken lines represent data obtained form the LIOAS measurements of this work.

value of $E_m(A_1^-/A_1)$ compares well to the expected range, where the lower limit is given by the E_m value of the excited donor P*-700 (approx. − 1300 meV) and the upper limit by $E(F_X^-/F_X) = -700$ meV [33].

From the energy storage of 65% in PS II particles we obtain a difference $E_m(Z^+/Z) - E_m(Q_A^-/Q_A)$ of 1190 meV. However, there is a well-known problem of heterogeneity in PS II quinone acceptor potentials [34]. Identifying Q_A with the so-called high potential Q (Q_H) and attributing to it an E_m value of typically −130 meV [34] results in an $E_m(Z^+/Z)$ of 1060 ± 100 meV. This compares reasonably well with the estimated value of 1 eV [35]. On the other hand, when choosing the value of $E_m(Q_L^-/Q_L) = -300$ meV typical for the low potential Q (Q_L) as reference value, we arrive at $E_m(Z^+/Z) = 850$ meV. This would not be sufficient to drive oxidation of water (at $E_m = 800$ meV) through the known series of intermediates [34]. Hence, we can conclude that the midpoint potential of Q_A is most likely that of Q_H and also similar to the midpoint potential of the primary quinone acceptor in isolated bacterial RCs.

Taking into account the possible Coulombic interaction between the positively charged donor and the negatively charged acceptor in the states Z^+-680IQ_A^- and P^+-700A_1^-, respectively, would generally have the consequence that the expected midpoint potential of (A_1^-/A_1) will be more negative and that of (Z^+/Z) more positive. The expected midpoint potential shifts could be in the order of up to 100 meV. Such a value can be calculated for static point charges when assuming a $Z^+ - Q_A^-$ distance in PS II of at least 3.2 nm (based on the $P - Q_A$ distance in bacterial RCs [36]) and a homogeneous dielectric with $\varepsilon_r = 4.5$. However, it is most likely that for RC complexes disintegrated from a membrane substantial electric depolarization has occurred already within our time window (a few μs). Hence, the Coulombic energy will be converted into heat and detected in our experiments. Therefore, the midpoint potential shift is probably negligible due to an almost complete dielectric relaxation of dipoles and charges within the microenvironment of Z^+ and Q_A^-. A similar conclusion has been derived in Refs. 16 and 28, where the standard free enthalpy

of the state $P^+Q_A^-$ in RCs and chromatophores of *Rhodobacter sphaeroides* was obtained by comparing the intensity of delayed and prompt fluorescence, respectively. A difference of 120 meV between the standard free enthalpy and the estimated midpoint potential difference was obtained for the chromatophores whereas no difference was obtained for the isolated RCs.

Acknowledgements

We thank I. Martin for programming and B. Kalka and U. Pieper for preparing the PS I and PS II particles. This work is part of the Ph.D. thesis of C.N. and is supported by a fellowship award to C.N. from the Alfried Krupp von Bohlen und Halbach-Stiftung, Essen. We are indebted to Professor K. Schaffner for his encouragement and support.

References

1 Parson, W.W. and Ke, B. (1982) in Photosynthesis, Vol. 1 (Govindjee, ed.), pp. 331–385, Academic Press, New York.
2 Van Gorkom, H.J. (1985) Photosynth. Res. 6, 97–112.
3 Rosencwaig, A. (1980) Photoacoustics and Photoacoustic Spectroscopy, Wiley, New York.
4 Malkin, S. and Cahen, D. (1979) Photochem. Photobiol. 29, 803–813.
5 Bults, G., Horwitz, B.A., Malkin, S. and Cahen, D. (1982) Biochim. Biophys. Acta 679, 452–465.
6 Carpentier, R., Larue, B. and Leblanc, R.M. (1984) Arch. Biochem. Biophys. 228, 534–543.
7 Poulet, P., Cahen, D. and Malkin, S. (1983) Biochim. Biophys. Acta 724, 433–446.
8 Canaani, O. and Malkin, S. (1984) Biochim. Biophys. Acta 766, 513–524.
9 Canaani, O. (1986) Biochim. Biophys. Acta 852, 74–80.
10 Patel, C.K.N. and Tam, A.C. (1981) Rev. Mod. Phys. 53, 517–550.
11 Lai, H.M. and Young, K. (1982) J. Acoust. Soc. Am. 72, 2000–2007.
12 Heihoff, K. and Braslavsky, S.E. (1986) Chem. Phys. Lett. 131, 183–188.
13 Jabben, M. and Schaffner, K. (1985) Biochim. Biophys. Acta 809, 445–451.
14 Yamaoka, T., Satoh, K. and Katoh, S. (1978) Plant Cell Physiol. 19, 943–954.
15 Schatz, G.H. and Witt, H.T. (1984) Photobiochem. Photobiophys. 7, 1–14.
16 Arata, H. and Parson, W.W. (1983) Biochim. Biophys. Acta 725, 394–401.
17 Dovichi, N.J. (1987) CRC Crit. Rev. Anal. Chem. 17, 357–424.
18 Braslavsky, S.E., Ellul, R.M., Weiss, R.G., Al-Ekabi, H. and Schaffner, K. (1983) Tetrahedron 39, 1909–1913.
19 Heihoff, K., Braslavsky, S.E. and Schaffner, K. (1987) Biochemistry 26, 1422–1427.
20 Tam, A.C. (1986) Rev. Mod. Phys. 58, 381–431.
21 Mörschel, E. and Schatz, G.H. (1987) Planta 172, 145–154.
22 Bonch-Bruevich, A.M., Razumova, T.K. and Starobogatow, I.O. (1977) Optics Spectrosc. 42, 45–48.
23 Mauzerall, D. (1976) J. Phys. Chem. 80, 2306–2309.
24 Bakker, J.G.C., Van Grondelle, R. and Den Hollander, W.T.F. (1983) Biochim. Biophys. Acta 725, 508–518.
25 Schatz, G.H., Brock, H. and Holzwarth, A.R. (1987) Proc. Natl. Acad. Sci. USA 84, 8414–8418.
26 Kramer, H. and Mathis, P. (1980) Biochim. Biophys. Acta 593, 319–329.
27 Rutherford, A.W. and Heathcote, P. (1985) Photosynth. Res. 6, 295–316.
28 Arata, H. and Parson, W.W. (1981) Biochim. Biophys. Acta 638, 201–209.
29 Schlodder, E., Brettel, K., Schatz, G.H. and Witt, H.T. (1984) Biochim. Biophys. Acta 765, 178–185.
30 Braslavsky, S.E. (1988) in Photoacoustic and Photothermal Phenomena (Hess, P. and Pelzl, J., eds.), pp. 508–513, Springer, Berlin.
31 Schatz, G.H. and Van Gorkom, H.J. (1985) Biochim. Biophys. Acta 810, 283–294.
32 Nanba, M. and Katoh, S. (1983) Biochim. Biophys. Acta 725, 272–279.
33 Chamarovsky, S.K. and Cammack, R. (1982) Photobiochem. Photobiophys. 4, 195–200.
34 Mathis, P. and Rutherford, A.W. (1987) in Photosynthesis (Amesz, J., ed.), pp. 63–96, Elsevier Science Publishers, Amsterdam.
35 Boussac, A. and Étienne, A.L. (1984) Biochim. Biophys. Acta 766, 576–581.
36 Deisenhofer, J., Epp, O., Miki, K., Huber, R. and Michel, H. (1984) J. Mol. Biol. 180, 385–398.
37 Schatz, G.H., Brock, H. and Holzwarth, A.R. (1988) Biophys. J., in press.